



PbSe quantum dot films with an enhanced electron mobility employed in hybrid polymer/nanocrystal solar cells

Journal:	<i>RSC Advances</i>
Manuscript ID	RA-ART-01-2016-001830.R1
Article Type:	Paper
Date Submitted by the Author:	02-Feb-2016
Complete List of Authors:	Zhang, Xiaoyu; Jilin University, Zhang, Yu; Jilin University, Wu, Hua; Jilin University, Yan, Long; Jilin University, Wang, Zhenguang; City University of Hong Kong, Department of Physics and Materials Science Zhao, Jun; Louisiana State University Shreveport, Yu, William; Rice University, Rogach, Andrey; City University of Hong Kong, Department of Physics and Materials Science
Subject area & keyword:	Solar energy < Energy

PbSe quantum dot films with an enhanced electron mobility employed in hybrid polymer/nanocrystal solar cells

Xiaoyu Zhang,^{ab} Yu Zhang,^{*a} Hua Wu,^a Long Yan,^a Zhenguang Wang,^b Jun Zhao,^{cd}
William W. Yu^{acd} and Andrey L. Rogach^{*b}

^aState Key Laboratory on Integrated Optoelectronics and College of Electronic Science and Engineering, Jilin University, Changchun 130012, China

^bDepartment of Physics and Materials Science and Centre for Functional Photonics (CFP), City University of Hong Kong, Kowloon, Hong Kong SAR

^cCollege of Material Science and Engineering, Qingdao University of Science and Technology, Qingdao 266042, China

^dDepartment of Chemistry and Physics, Louisiana State University, Shreveport, LA 71115, USA

* Corresponding authors. E-mails: yuzhang@jlu.edu.cn (Yu Zhang).

andrey.rogach@cityu.edu.hk (Andrey L. Rogach)

Abstract

We explore two strategies to improve the performance of hybrid solar cells fabricated using poly (3-hexylthiophene) (P3HT) and colloidal PbSe nanocrystals, which have reached a 1 sun power conversion efficiency of 2.9 %. Using atomic passivation strategy towards inorganic ligand-capped nanocrystals, the electron mobilities of PbSe quantum dot films are improved from $1.95 \times 10^{-6} \text{ cm}^2 \text{V}^{-1} \text{s}^{-1}$ to $1.15 \times 10^{-5} \text{ cm}^2 \text{V}^{-1} \text{s}^{-1}$. Employing ultras-small PbSe nanocrystals allows us to adjust their bandgaps towards the type II heterojunction with P3HT, thus achieving efficient charge separation and transfer between the polymer/inorganic constituents. The device performance dropped to its half after 10 days' storage, and the P3HT/PbSe interface was found to play a primary role in this efficiency degradation.

Key words: hybrid solar cells, PbSe nanocrystals, poly (3-hexylthiophene), electron mobility, atomic passivation

1 Introduction

Solution processed polymer-based solar cells have been widely studied due to the prospects of low-cost scalable roll-to-roll manufacturing and high optical absorbance of conjugated polymers.¹⁻⁶ In these devices, the polymer acting as an electron donor is commonly blended with the fullerene derivative acting as an electron acceptor. However, fullerene-based acceptor materials usually exhibit a weak absorbance, which limits the device performance.^{7,8} In order to address this issue, employment of inorganic semiconductor nanocrystals (NCs) as acceptor materials with easily tunable bandgaps to replace the fullerene derivative attracted much attention in recent years.⁹⁻¹² Since the first conjugated polymer-NC solar cell was reported by Alivisatos and co-workers in 2002,¹³ hybrid solar cells (HSCs) of this kind have been widely investigated, and continuous increase in their power conversion efficiencies (PCEs) has been achieved, which is enabled by both new device architecture and improvements in materials.¹⁴ For example, Yang *et al.* fabricated HSCs based on aqueous CdTe NCs and poly(p-phenylenevinylene), with a PCE of 4.7%.¹⁵ Xue *et al.* achieved a PCE approaching 5% for HSCs based on CdSe NCs and a low band-gap polymer PCPDTBT.¹⁶ Recently, Ma *et al.* reported the PCE of 5.5% by employing $\text{PbS}_x\text{Se}_{1-x}$ alloy NCs and optimizing device architecture of HSCs.¹⁷

Comparing to fullerene derivatives, semiconductor NCs possess several advantages as acceptor materials, such as large absorption coefficients and easily tuned energy levels.

At the same time, achieving high charge mobilities in semiconductor quantum dot films is often a challenge,¹⁸⁻²⁰ which has been addressed in the recent years by designing short inorganic-based ligands²¹⁻²³ or treatment with halides.²⁴⁻²⁶ Till now, most of the reported HSCs were based on the combination of conducting polymers and cadmium chalcogenide NCs,²⁷⁻³³ and thus were able to harvest only visible light. To better utilize the near-infrared (NIR) region of the solar spectrum, lead chalcogenide NCs such as PbS and PbSe were introduced into HSCs.³⁴⁻³⁶ Benefiting from the large bulk Bohr radius in lead chalcogenides, the quantum confinement in these colloidal NCs allows the bandgap and the absorption edge to be tuned across the entire NIR spectrum.³⁷ PbSe NC-based solar cells have previously shown stable performance without encapsulation for over 50 days in ambient conditions.³⁸ Furthermore, PbSe NCs have been reported to exhibit a multiple exciton generation (MEG) effect, which has been confirmed for the solar cell with a peak external quantum efficiency of 114%.³⁹ Not only the MEG effect has been observed in several kinds of NC materials, but it has also been demonstrated in PbS, PbSe, PbTe and CuInSe₂ NC-based solar cells,³⁹⁻⁴³ meaning that these nanoscale materials have great potential to exceed the Shockley-Queisser limit and approach the Ross-Nozik limit.⁴⁴ Another reason for using PbSe rather than PbS NCs is related to the possibility of realization of an efficient type-II heterojunction between P3HT and a polymer, as PbSe NCs possess deeper-lying HOMO energies than the same sized PbS NCs.⁴⁵

Even though high mobility values up to $0.3 \text{ cm}^2\text{V}^{-1}\text{s}^{-1}$ and $10 \text{ cm}^2\text{V}^{-1}\text{s}^{-1}$ have been

reported for holes and electrons in PbSe NC films,^{46, 47} rather modest PCE values been achieved so far in the related devices.^{17, 48-51} In this work, we addressed this issue for the HSCs employing polymer poly(3-hexylthiophene) (P3HT) and PbSe NCs. By using monovalent halide anions to replace the surface ligands of PbSe NCs,²⁴ we enhanced the electron mobility of PbSe films. Through tuning the NC bandgap *via* the quantum size effect, type II band-offsets were realized between PbSe NCs and P3HT polymer. In order to explore the potential of the type II heterojunction, we employed a layer by layer processed planar junction structure, and achieved PCE values of up to 2.9 %, a ten-fold increase compared to the previously reported value of 0.26 % for P3HT/PbSe NC based devices.⁵⁰

2 Methods

The synthesis of PbSe NCs

PbSe NCs were synthesized following the previously reported method.^{52, 53} Lead(II) oxide (Aladdin, 99.99%, 0.892 g), oleic acid (Alfa Aesar, 90%, 5 ml) and 1-octadecene (Alfa Aesar, 90%, 12 ml) were loaded into a three-neck flask equipped with a condenser, magnetic stirrer, thermocouple, and heating mantle. The reaction mixture was heated to 180°C under N₂ flow for 1h until the solution turned colorless. After the solution was cooled to 90°C, 8 mL of 1.0 M Se-tributylphosphine was rapidly injected into the reaction flask. The NCs were grown at 75°C for a desired time (ranging from 180 to 460 s) to achieve the average quantum dot size ranging

from 2.3 to 2.9 nm, with the position of the first excitonic maximum (a measure for the NC bandgap) ranging from 1.50 eV to 1.35 eV as listed in Table 1. The reaction was rapidly quenched by injection of 50 ml of methanol, the PbSe NCs were purified by precipitation in octane/methanol and in octane/butyl alcohol, dissolved in octane and stored in a N₂-filled glove box for the device fabrication.

ZnO NCs Synthesis

ZnO NCs used for the fabrication of the electron transport layer were synthesized based on the previously reported method.⁵⁴ Zinc acetate (Aldrich, 99.99%, 0.4403 g) and 30 mL of ethyl alcohol were loaded into a 250 mL three-neck flask and heated to 75°C under N₂ flow until a clear solution was obtained. The reaction solution was cooled to room temperature, and 10 mL of a sodium hydroxide (Alfa Aesar, 98%, 0.2g)/ethyl alcohol solution was injected into the flask. The solution was stirred for 4h, ZnO NCs were purified by precipitation in hexane and in ethanol/hexane, dissolved in ethanol and stored in a N₂-filled glove box for the device fabrication.

Device fabrication

Patterned ITO substrates were cleaned with soap, deionized water, ethanol, chloroform, acetone, and isopropanol followed by treatment with oxygen plasma. A thin layer of PEDOT:PSS (~40 nm) was deposited on the ITO substrate, followed by annealing at 150°C for 10 min in air. The substrate was transferred into a N₂-filled glove box, and a P3HT layer (~40 nm) was deposited by a spin-coating of 15 mg/mL

P3HT solution in methylbenzene, followed by annealing at 100°C for 10 min. Multiple PbSe NC layers (~80nm total thickness) were fabricated by layer-by-layer spin-coating. For each single layer, PbSe NC solution (12 mg/ml) in octane was spin-cast onto the substrate, and a cetyltrimethylammonium bromide solution (CTAB, 10 mg/ml in methanol) was then applied to the substrate for 30 s, followed by three rinse-spin steps with methanol. For the respective treatment of PbSe NCs with ethanedithiol (EDT) its 0.02 vol% solution in acetonitrile has been used. ZnO layers (20 nm) were fabricated by a spin-coating of a solution (6.5 mg/ml) of ZnO nanoparticles. Al electrodes (100nm thick) were thermally evaporated onto the films through a shadow mask at a pressure of 10^{-6} mbar. The nominal device areas were defined by the overlap of the anode and cathode and constituted 4 mm².

Characterization

Fourier transform infrared (FTIR) spectra were measured on a Bruker Tensor 27 spectrometer. Absorption and photoluminescence (PL) spectra were collected on a Perkin-Elmer Lambda 950 UV-vis spectrophotometer and a Perkin-Elmer LS50B spectrofluorimeter, respectively. Current-voltage characteristics of the solar cells in the dark and under light were measured using a Keithley 2612B source meter. The 1 sun illumination from the solar simulator was determined using a calibrated single-crystalline silicon reference cell.

3 Results and discussion

Electron acceptors for solar cell applications require high electron mobilities. Ligand exchange is an efficient strategy in reducing the inter-particle distance and enhancing carrier transportation, and the most commonly employed one is the EDT treatment, which would replace the long organic chains (8-18 carbons) on NC surface by short organic ligands (~ 0.5 nm). Recently, another strategy for the surface ligand exchange on colloidal quantum dots has evolved, which involve halide anions like Br^- offering even shorter interparticle distances. The success of this so-called atomic-ligand passivation has been already demonstrated for a number of NCs.^{24, 25, 55} In this work, we applied both strategies, EDT and bromide (using CTAB) treatments to improve the electron mobilities of PbSe NC films. FTIR spectra shown in Figure 1a indicate the complete removal of the oleate ligands for both EDT and CTAB treated PbSe NC films, whose C-H vibrations at $2,922\text{ cm}^{-1}$ and $2,852\text{ cm}^{-1}$, and COO^- vibrations at $1,545\text{ cm}^{-1}$ and $1,403\text{ cm}^{-1}$, were all eliminated as a result of the treatment. To estimate the influence of different ligand treatments on the electron mobilities of PbSe NC films, electron-only devices in configuration of ITO/PEI/NCs/PEI/Al were fabricated and characterized. The PEI (polyethylenimine) is a polymer containing aliphatic amine groups, which is commonly employed in reducing the work function of a conductor material.⁵⁶ Current density-voltage (J-V) characteristics of devices based on PbSe NCs with a CTAB or EDT treatment are presented in Figure 1b, testifying the greatly improved charge transport properties for the CTAB treated NC films. Based on the space charge-limited current (SCLC) model and the Mott-Gurney law, the

charge mobility μ can be calculated from:

$$J = \frac{9}{8} \epsilon_0 \epsilon_r \mu \frac{V^2}{L^3}$$

where $\epsilon_0 \epsilon_r$ ($\epsilon_r = 250$ here)⁵⁷ is the dielectric permittivity of the PbSe NC film; L is the thickness of the PbSe NC film; J is the current density; and V is the applied voltage. From the fitting of the J-V curves of Figure 1b based on the above expression, the electron mobility of PbSe NC films increased from $1.95 \times 10^{-6} \text{ cm}^2 \text{V}^{-1} \text{s}^{-1}$ (EDT treatment) to $1.15 \times 10^{-5} \text{ cm}^2 \text{V}^{-1} \text{s}^{-1}$ (CTAB treatment). These values were smaller than previously reported mobilities for PbSe NC films,⁵⁸ which was due to the smaller sizes of NCs we have employed.

HSCs benefit from the type II heterojunction between the donor/acceptor constituents.⁵⁹ As commonly used polymer components of HSCs like P3HT have a higher lowest unoccupied molecular orbital (LUMO) energy than that of PbSe NCs, they can easily serve as donor transferring electrons to NC acceptors, while the ability for photoexcited holes to be transferred from PbSe NCs to P3HT may present a shortcoming for certain NC sizes. We have used ultrasmall PbSe NCs (size range 2.3-2.9 nm) with the highest occupied molecular orbital (HOMO) energy levels around -5.4 eV to ensure formation of the type II band-offset in contact with P3HT. This is proven by solution-state PL quenching measurements which are a common method to examine the energy level arrangement at the NC-polymer interface.⁶⁰⁻⁶² The comparison of PL intensity for bare PbSe NCs and blends of PbSe NCs with P3HT (1:1wt%) in the NIR region is presented in Figure 2a for two NCs sizes, namely

2.6 and 2.9 nm. PL quenching has been observed for both NC sizes, indicating the efficient hole transfer from NCs to P3HT. The PL quenching was stronger for smaller (2.6 nm) PbSe NCs than for the larger (2.9 nm) ones, due to the larger difference between the respective HOMO energies in the former case. The electron transfer from the photo-excited state of P3HT to the LUMO of PbSe Ns can be estimated from the quenching of the emission of P3HT in the visible spectral region, as presented in Figure 2b. Compared to the PL intensity of P3HT solution, PL quenching was observed for P3HT blended with PbSe NCs of the both sizes, 2.6 nm and 2.9 nm. Taken together, these results point out on the formation of a type II band-offset between ultrasmall PbSe NCs and P3HT, being energetically favorable for the efficient exciton dissociation at their interface.

To explore the potential of the type II heterojunction between P3HT and PbSe NCs, a planar junction configuration was employed, with the corresponding HSC device structure shown in Figure 3a. The energy level alignment of this device (based on values provided in Refs. ^{36,54}) is shown in Figure 3b. As PbSe NCs have large exciton diffusion length on the order of 100 nm, PbSe films with the thickness of 80 nm were fabricated.⁶³ The PEDOT:PSS and the ZnO NC films were used as the hole / electron extraction layers, and at the same time electron / hole blocking layers, respectively. Absorption spectra of P3HT, ZnO NCs, and PbSe NCs with different particle sizes employed in this study are presented in Figure 3c and 3d. The average particle sizes of PbSe NCs referred to in this work have been estimated from the sizing equation of

Ref. ⁶⁴ based on the position of the first excitonic maximum in their absorption spectra as in Figure 3d.

J-V curves for the HSCs based on PbSe NC films treated with EDT or CTAB are shown in Figure 4a. The EDT treated devices exhibited a short-circuit current (J_{SC}) of 10.62 mA/cm², open-circuit voltage (V_{OC}) of 0.38 V, fill factor (FF) of 40%, and PCE of 1.62%. The CTAB treated devices exhibited a J_{SC} of 11.51 mA/cm², V_{OC} of 0.56 V, FF of 45%, and PCE of 2.90%. All these parameters have been improved as a result of the CTAB treatment as compared to the EDT, manifesting in a 79% improvement of PCE. The J_{SC} of a planar solar cell is commonly associated with the mobility of the active layer material, with a higher mobility resulting in a higher J_{SC} .²⁴ Nearly 5-fold increase in the electron mobility for the CTAB treated PbSe NC film as compared to that of the EDT treated NC film (Figure 1b) may be responsible to the higher J_{SC} for this kind of cells. In a traditional heterojunction diode solar cell, the V_{OC} is determined by the difference in the location of the Fermi levels between the electron donor and the electron acceptor film (the built-in junction potential, V_{bi}).⁶⁵ The properties of the electron acceptor in HSC under study depend on both NC size and the surface chemistry, and their surface modification with different ligands may result in different kind of electronic conductivity.^{58, 66} PbSe NC film showed ambipolar conductance after EDT treatment,⁶⁷ but performed as n-type semiconductors after CTAB treatment,⁶⁸ so that different kinds of devices can be obtained when combining them with p-type P3HT films. Figure 5b shows energy band diagrams for P3HT/PbSe

NC heterojunctions where PbSe NC films are either intrinsic (EDT treatment) or n-doped (as a result of CTAB treatment). For the EDT-treated films, the Fermi level (E_F) is positioned midway between the HOMO and LUMO of PbSe NCs. For the n-type CTAB-treated NC film, the E_F would shift up and get close to the LUMO of PbSe NCs. The V_{bi} here is the difference in the location of Fermi levels between P3HT and PbSe NC film. Since the E_F in P3HT is close to its HOMO and independent of the doping of PbSe NC films, the $V_{bi-CTAB}$ value is higher than V_{bi-EDT} , which causes the difference in V_{OC} values in the related solar cell structure studied here (Figure 4a).

To evaluate the HSC performance as a function of size and thus the optical bandgap of PbSe NCs, a series of devices employed CTAB treated NCs with three different sizes and thus the location of first excitonic peaks of 1.35 eV (2.9 nm diameter), 1.42 eV (2.6nm), and 1.50 eV (2.3 nm) were fabricated. The J-V characteristics of these solar cells are presented in Figure 4b, with the average photovoltaic parameters out of 16 devices summarized in Table 1. A fundamental trade-off between the V_{OC} and J_{SC} was observed for devices employing NC of different sizes. The V_{OC} increased from 0.38 to 0.59 V for NCs whose first excitonic maximum changed from 1.35 to 1.50 eV, while the J_{SC} decreased from 14.1 to 4.9 mA/cm². The bandgap of PbSe NCs changes with the NC size due to the quantum confinement, with smaller NCs possessing larger bandgaps.⁶⁹ For n-type PbSe NC films, an increase in the bandgap of the NCs shifts the NC Fermi level up,⁶⁵ which causes an increase of the V_{bi} values, resulting in

higher V_{OC} . At the same time, smaller PbSe NCs suffer from the reduced absorption in the NIR region of the solar energy, resulting in a lower J_{SC} . Besides, the loss of current may also originate from lower mobilities of smaller PbSe NCs. Reduced mobilities have been reported as a result of decreasing PbSe NC sizes,^{70, 71} which may be a result of more interparticle hops needed for a photogenerated charge to traverse the film, increased surface area, and/or increased depth of localized trap energies as the band edges move farther away with confinement. We have also performed SCLC measurements on our samples to address this point; as shown in Figure 4d, the mobilities for 2.9, 2.6, and 2.3 nm PbSe NC films are 2.24×10^{-5} , 1.11×10^{-5} , and $4.23 \times 10^{-6} \text{ cm}^2 \text{V}^{-1} \text{s}^{-1}$, respectively. As a result, we have achieved the highest photovoltaic performance for HSCs employing PbSe NCs with the intermediate size of 2.6 nm.

Stability of HSCs were evaluated by measuring J-V curves of the devices employing 2.6 nm PbSe NCs stored in a N_2 -filled glove box for a period of up to 30 days. Variations of photovoltaic performance parameters during this period of time are summarized in Figure 5. While V_{OC} only experienced slight degradation, other parameters decreased rapidly. The PCE of the device reduced below 50 % of the initial value after 10 days of storage. Since PCE values for devices without PbSe NC layers (ITO/PEDOT:PSS/P3HT:ZnO/ZnO/Al) remained unchanged even after 80 days,⁷² the efficiency loss in our devices was most probably related to the PbSe/ZnO or P3HT/PbSe interfaces. For the PbSe/ZnO interface, fewer intragap states exist in

the contact region,⁷³ and devices based on these two materials have also shown stability over 50 days.³⁸ Thus we make a conclusion that it was the P3HT/PbSe interface which played a primary role in the device efficiency degradation.

4 Conclusions

By using monovalent halide anions to replace the surface ligands of PbSe NCs, we enhanced the electron mobility of PbSe quantum dot based films. We designed a type II heterojunction solar cells employing very small PbSe NCs and P3HT, where both the high electron mobility of the PbSe NC film and the improved charge transfer efficiency between the P3HT polymer and NCs resulted in a PCE of 2.9 %, which is very close to that of a P3HT and (6, 6)-phenyl C₆₁-butyric acid methyl ester (PC₆₁BM) based device.⁷⁴ This indicates an ample potential of PbSe NCs as an electron acceptor component in the hybrid polymer/nanocrystal solar cells.

Acknowledgements

This work was financially supported by the National Natural Science Foundation of China (51272084, 61306078, 61225018, 61475062), the Jilin Province Key Fund (20140204079GX), Research Fund for the Doctoral Program of Higher Education (20130061110046), the Opened Fund of the State Key Laboratory on Integrated Optoelectronics (IOSKL2014KF14), and the Research Grant Council of Hong Kong

S.A.R. (T23-713/11).

References

- 1 X. Guo, N. Zhou, S. J. Lou, J. Smith, D. B. Tice, J. W. Hennek, R. P. Ortiz, J. T. L. Navarrete, S. Li, J. Strzalka, L. X. Chen, R. P. H. Chang, A. Facchetti and T. J. Marks, *Nat. Photon.*, 2013, **7**, 825-833.
- 2 D. Ginley, M. A. Green and R. Collins, *MRS Bull.*, 2008, **33**, 355-364.
- 3 A. C. Mayer, S. R. Scully, B. E. Hardin, M. W. Rowell and M. D. McGehee, *Mater. Today*, 2007, **10**, 28-33.
- 4 H. Spanggaard and F. C. Krebs, *Sol. Energy Mater. Sol. Cells*, 2004, **83**, 125-146.
- 5 M. Graetzel, R. A. J. Janssen, D. B. Mitzi and E. H. Sargent, *Nature*, 2012, **488**, 304-312.
- 6 S. R. Forrest, *Nature*, 2004, **428**, 911-918.
- 7 M. D. Diener and J. M. Alford, *Nature*, 1998, **393**, 668-671.
- 8 Y. He and Y. Li, *Phys. Chem. Chem. Phys.*, 2011, **13**, 1970-1983.
- 9 M. Eck, C. V. Pham, S. Zufle, M. Neukom, M. Sessler, D. Scheunemann, E. Erdem, S. Weber, H. Borchert, B. Ruhstaller and M. Kruger, *Phys. Chem. Chem. Phys.*, 2014, **16**, 12251-12260.
- 10 A. Lefrançois, B. Luszczynska, B. Pepin-Donat, C. Lombard, B. Bouthinon, J.-M. Verilhac, M. Gromova, J. Faure-Vincent, S. Pouget, F. Chandezon, S. Sadki and P. Reiss, *Sci. Rep.*, 2015, **5**, 7768.
- 11 Y. Zhou, M. Eck, C. Veit, B. Zimmermann, F. Rauscher, P. Niyamakom, S.

- Yilmaz, I. Dumsch, S. Allard, U. Scherf and M. Krüger, *Sol. Energy Mater. Sol. Cells*, 2011, **95**, 1232-1237.
- 12 M. J. Greaney and R. L. Brutchey, *Mater. Today*, 2015, **18**, 31-38.
- 13 W. U. Huynh, J. J. Dittmer and A. P. Alivisatos, *Science*, 2002, **295**, 2425-2427.
- 14 Z. Chen, H. Zhang, W. Yu, Z. Li, J. Hou, H. Wei and B. Yang, *Adv. Energy Mater.*, 2013, **3**, 433-437.
- 15 Z. Chen, H. Zhang, X. Du, X. Cheng, X. Chen, Y. Jiang and B. Yang, *Energy Environ. Sci.*, 2013, **6**, 1597-1603.
- 16 R. Zhou, R. Stalder, D. Xie, W. Cao, Y. Zheng, Y. Yang, M. Plaisant, P. H. Holloway, K. S. Schanze, J. R. Reynolds and J. Xue, *ACS Nano*, 2013, **7**, 4846-4854.
- 17 Z. Liu, Y. Sun, J. Yuan, H. Wei, X. Huang, L. Han, W. Wang, H. Wang and W. Ma, *Adv. Mater.*, 2013, **25**, 5772-5778.
- 18 F. Hetsch, N. Zhao, S. V. Kershaw and A. L. Rogach, *Mater. Today*, 2013, **16**, 312-325.
- 19 M. Chen, L. Shao, S. V. Kershaw, H. Yu, J. Wang, A. L. Rogach and N. Zhao, *ACS Nano*, 2014, **8**, 8208-8216.
- 20 M. Chen, H. Yu, S. V. Kershaw, H. Xu, S. Gupta, F. Hetsch, A. L. Rogach and N. Zhao, *Adv. Funct. Mater.*, 2014, **24**, 53-59.
- 21 J. Huang, W. Liu, D. S. Dolzhenko, L. Protesescu, M. V. Kovalenko, B. Koo, S. Chattopadhyay, E. V. Shchenchenko and D. V. Talapin, *ACS Nano*, 2014, **8**,

- 9388-9402.
- 22 H. Zhang, J. Jang, W. Liu and D. V. Talapin, *ACS Nano*, 2014, **8**, 7359-7369.
- 23 W. Liu, J.-S. Lee and D. V. Talapin, *J. Am. Chem. Soc.*, 2013, **135**, 1349-1357.
- 24 J. Tang, K. W. Kemp, S. Hoogland, K. S. Jeong, H. Liu, L. Levina, M. Furukawa, X. Wang, R. Debnath, D. Cha, K. W. Chou, A. Fischer, A. Amassian, J. B. Asbury and E. H. Sargent, *Nat. Mater.*, 2011, **10**, 765-771.
- 25 A. H. Ip, S. M. Thon, S. Hoogland, O. Voznyy, D. Zhitomirsky, R. Debnath, L. Levina, L. R. Rollny, G. H. Carey, A. Fischer, K. W. Kemp, I. J. Kramer, Z. Ning, A. J. Labelle, K. W. Chou, A. Amassian and E. H. Sargent, *Nat Nano*, 2012, **7**, 577-582.
- 26 Z. Ning, Y. Ren, S. Hoogland, O. Voznyy, L. Levina, P. Stadler, X. Lan, D. Zhitomirsky and E. H. Sargent, *Adv. Mater.*, 2012, **24**, 6295-6299.
- 27 Y. Zhou, M. Eck, C. Men, F. Rauscher, P. Niyamakom, S. Yilmaz, I. Dumsch, S. Allard, U. Scherf and M. Krüger, *Sol. Energy Mater. Sol. Cells*, 2011, **95**, 3227-3232.
- 28 P. Reiss, E. Couderc, J. De Girolamo and A. Pron, *Nanoscale*, 2011, **3**, 446-489.
- 29 H.-C. Chen, C.-W. Lai, I. C. Wu, H.-R. Pan, I. W. P. Chen, Y.-K. Peng, C.-L. Liu, C.-h. Chen and P.-T. Chou, *Adv. Mater.*, 2011, **23**, 5451-5455.
- 30 W. Fu, L. Wang, Y. Zhang, R. Ma, L. Zuo, J. Mai, T.-K. Lau, S. Du, X. Lu, M. Shi, H. Li and H. Chen, *ACS Appl. Mater. Interfaces*, 2014, **6**, 19154-19160.
- 31 M. J. Greaney, J. Araujo, B. Burkhart, B. C. Thompson and R. L. Brutchey,

- Chem. Commun.*, 2013, **49**, 8602-8604.
- 32 K. F. Jeltsch, M. Schädel, J.-B. Bonekamp, P. Niyamakom, F. Rauscher, H. W. A. Lademann, I. Dumsch, S. Allard, U. Scherf and K. Meerholz, *Adv. Funct. Mater.*, 2012, **22**, 397-404.
- 33 M. Pientka, V. Dyakonov, D. Meissner, A. Rogach, D. Talapin, H. Weller, L. Lutsen and D. Vanderzande, *Nanotechnology*, 2004, **15**, 163.
- 34 H.-Y. Chen, J. Hou, S. Dayal, L. Huo, N. Kopidakis, M. C. Beard and J. M. Luther, *Adv. Energy Mater.*, 2011, **1**, 528-533.
- 35 K. M. Noone, E. Strein, N. C. Anderson, P.-T. Wu, S. A. Jenekhe and D. S. Ginger, *Nano Lett.*, 2010, **10**, 2635-2639.
- 36 J. Yuan, A. Gallagher, Z. Liu, Y. Sun and W. Ma, *J. Mater. Chem. A*, 2015, **3**, 2572-2579.
- 37 F. W. Wise, *Acc. Chem. Res.*, 2000, **33**, 773-780.
- 38 S. Kim, A. R. Marshall, D. M. Kroupa, E. M. Miller, J. M. Luther, S. Jeong and M. C. Beard, *ACS Nano*, 2015, **9**, 8157-8164.
- 39 O. E. Semonin, J. M. Luther, S. Choi, H.-Y. Chen, J. Gao, A. J. Nozik and M. C. Beard, *Science*, 2011, **334**, 1530-1533.
- 40 M. L. Böhm, T. C. Jellicoe, M. Tabachnyk, N. J. L. K. Davis, F. Wisnivesky-Rocca-Rivarola, C. Ducati, B. Ehrler, A. A. Bakulin and N. C. Greenham, *Nano Lett.*, 2015, **15**, 7987-7993.
- 41 N. J. L. K. Davis, M. L. Bohm, M. Tabachnyk, F. Wisnivesky-Rocca-Rivarola, T. C. Jellicoe, C. Ducati, B. Ehrler and N. C. Greenham, *Nat Commun*, 2015,

6.

- 42 J. B. Sambur, T. Novet and B. A. Parkinson, *Science*, 2010, **330**, 63-66.
- 43 C. J. Stolle, T. B. Harvey, D. R. Pernik, J. I. Hibbert, J. Du, D. J. Rhee, V. A. Akhavan, R. D. Schaller and B. A. Korgel, *J. Phys. Chem. L*, 2014, **5**, 304-309.
- 44 R. T. Ross and A. J. Nozik, *J. Appl. Phys.*, 1982, **53**, 3813-3818.
- 45 B.-R. Hyun, Y.-W. Zhong, A. C. Bartnik, L. Sun, H. D. Abruña, F. W. Wise, J. D. Goodreau, J. R. Matthews, T. M. Leslie and N. F. Borrelli, *ACS Nano*, 2008, **2**, 2206-2212.
- 46 M. Scheele, J. H. Engel, V. E. Ferry, D. Hanifi, Y. Liu and A. P. Alivisatos, *ACS Nano*, 2013, **7**, 6774-6781.
- 47 S. J. Oh, N. E. Berry, J.-H. Choi, E. A. Gaulding, T. Paik, S.-H. Hong, C. B. Murray and C. R. Kagan, *ACS Nano*, 2013, **7**, 2413-2421.
- 48 D. Cui, J. Xu, T. Zhu, G. Paradee, S. Ashok and M. Gerhold, *Appl. Phys. Lett.*, 2006, **88**, 183111.
- 49 X. Jiang, R. D. Schaller, S. B. Lee, J. M. Pietryga, V. I. Klimov and A. A. Zakhidov, *J. Mater. Res.*, 2007, **22**, 2204-2210.
- 50 Z. Tan, T. Zhu, M. Thein, S. Gao, A. Cheng, F. Zhang, C. Zhang, H. Su, J. Wang, R. Henderson, J.-i. Hahm, Y. Yang and J. Xu, *Appl. Phys. Lett.*, 2009, **95**, 063510.
- 51 Y. Sun, Z. Liu, J. Yuan, J. Chen, Y. Zhou, X. Huang and W. Ma, *Org. Electron.*, 2015, **24**, 263-271.

- 52 C. M. Evans, L. Guo, J. J. Peterson, S. Maccagnano-Zacher and T. D. Krauss, *Nano Lett.*, 2008, **8**, 2896-2899.
- 53 W. W. Yu, J. C. Falkner, B. S. Shih and V. L. Colvin, *Chem. Mater.*, 2004, **16**, 3318-3322.
- 54 X. Zhang, Y. Zhang, L. Yan, C. Ji, H. Wu, Y. Wang, P. Wang, T. Zhang, Y. Wang, T. Cui, J. Zhao and W. W. Yu, *J. Mater. Chem. A*, 2015, **3**, 8501-8507.
- 55 D. C. J. Neo, C. Cheng, S. D. Stranks, S. M. Fairclough, J. S. Kim, A. I. Kirkland, J. M. Smith, H. J. Snaith, H. E. Assender and A. A. R. Watt, *Chem. Mater.*, 2014, **26**, 4004-4013.
- 56 Y. Zhou, C. Fuentes-Hernandez, J. Shim, J. Meyer, A. J. Giordano, H. Li, P. Winget, T. Papadopoulos, H. Cheun, J. Kim, M. Fenoll, A. Dindar, W. Haske, E. Najafabadi, T. M. Khan, H. Sojoudi, S. Barlow, S. Graham, J.-L. Brédas, S. R. Marder, A. Kahn and B. Kippelen, *Science*, 2012, **336**, 327-332.
- 57 D. V. Talapin and C. B. Murray, *Science*, 2005, **310**, 86-89.
- 58 M. H. Zarghami, Y. Liu, M. Gibbs, E. Gebremichael, C. Webster and M. Law, *ACS Nano*, 2010, **4**, 2475-2485.
- 59 N. Yaacobi-Gross, N. Garphunkin, O. Solomeshch, A. Vaneski, A. S. Susha, A. L. Rogach and N. Tessler, *ACS Nano*, 2012, **6**, 3128-3133.
- 60 Y. Zhang, Z. Li, J. Ouyang, S.-W. Tsang, J. Lu, K. Yu, J. Ding and Y. Tao, *Org. Electron.*, 2012, **13**, 2773-2780.
- 61 M. Nam, T. Lee, S. Kim, S. Kim, S.-W. Kim and K.-K. Lee, *Org. Electron.*, 2014, **15**, 391-398.

- 62 A. A. Lutich, G. Jiang, A. S. Susha, A. L. Rogach, F. D. Stefani and J. Feldmann, *Nano Lett.*, 2009, **9**, 2636-2640.
- 63 J. M. Luther, M. Law, M. C. Beard, Q. Song, M. O. Reese, R. J. Ellingson and A. J. Nozik, *Nano Lett.*, 2008, **8**, 3488-3492.
- 64 Q. Dai, Y. Wang, X. Li, Y. Zhang, D. J. Pellegrino, M. Zhao, B. Zou, J. Seo, Y. Wang and W. W. Yu, *ACS Nano*, 2009, **3**, 1518-1524.
- 65 K. S. Leschkies, T. J. Beatty, M. S. Kang, D. J. Norris and E. S. Aydil, *ACS Nano*, 2009, **3**, 3638-3648.
- 66 P. R. Brown, D. Kim, R. R. Lunt, N. Zhao, M. G. Bawendi, J. C. Grossman and V. Bulović, *ACS Nano*, 2014, **8**, 5863-5872.
- 67 J. M. Luther, M. Law, Q. Song, C. L. Perkins, M. C. Beard and A. J. Nozik, *ACS Nano*, 2008, **2**, 271-280.
- 68 Z. Ning, O. Voznyy, J. Pan, S. Hoogland, V. Adinolfi, J. Xu, M. Li, A. R. Kirmani, J.-P. Sun, J. Minor, K. W. Kemp, H. Dong, L. Rollny, A. Labelle, G. Carey, B. Sutherland, I. Hill, A. Amassian, H. Liu, J. Tang, O. M. Bakr and E. H. Sargent, *Nat Mater*, 2014, **13**, 822-828.
- 69 J. J. Choi, Y.-F. Lim, M. E. B. Santiago-Berrios, M. Oh, B.-R. Hyun, L. Sun, A. C. Bartnik, A. Goedhart, G. G. Malliaras, H. D. Abruña, F. W. Wise and T. Hanrath, *Nano Lett.*, 2009, **9**, 3749-3755.
- 70 W. Ma, S. L. Swisher, T. Ewers, J. Engel, V. E. Ferry, H. A. Atwater and A. P. Alivisatos, *ACS Nano*, 2011, **5**, 8140-8147.
- 71 Y. Liu, M. Gibbs, J. Puthussery, S. Gaik, R. Ihly, H. W. Hillhouse and M. Law,

Nano Lett., 2010, **10**, 1960-1969.

- 72 S. Venkataprasad Bhat, A. Govindaraj and C. N. R. Rao, *Sol. Energy Mater. Sol. Cells*, 2011, **95**, 2318-2321.
- 73 B. Ehrler, K. P. Musselman, M. L. Böhm, F. S. F. Morgenstern, Y. Vaynzof, B. J. Walker, J. L. MacManus-Driscoll and N. C. Greenham, *ACS Nano*, 2013, **7**, 4210-4220.
- 74 M. T. Dang, L. Hirsch and G. Wantz, *Adv. Mater.*, 2011, **23**, 3597-3602.

Table 1. Summary of photovoltaic performance of HSCs listed as a function of the PbSe NC size and their first exciton energy

NC diameter (nm)	Exciton energy (eV)	V _{OC} (V)	J _{SC} (mA cm ⁻²)	FF (%)	PCE (%)
2.9	1.35	0.38±0.02	14.1±2.3	36±5	1.94±0.3
2.6	1.42	0.55±0.01	11.5±1.6	40±5	2.52±0.4
2.3	1.50	0.59±0.01	4.89±0.9	32±3	0.93±0.2

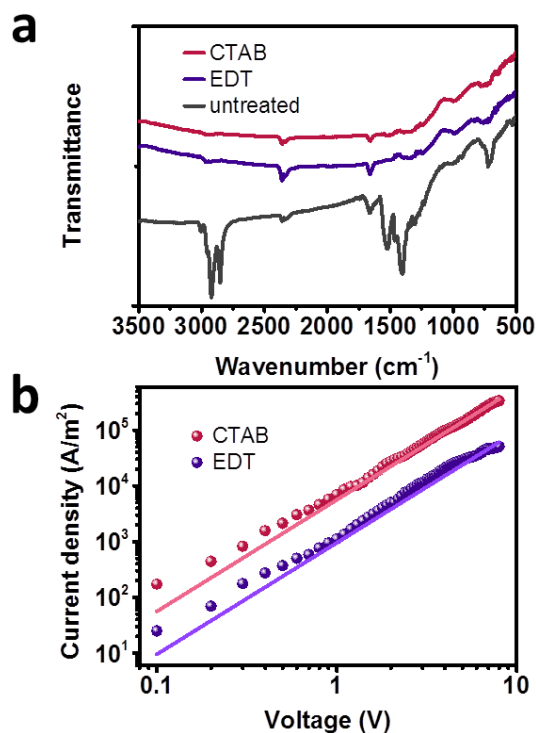


Figure 1. (a) FTIR spectra of PbSe NC films treated by CTAB and EDT. Vibrations at 2922 cm⁻¹ and 2852 cm⁻¹ are ν_{asym} (C-H) and ν_{sym} (C-H), and vibrations at 1545 cm⁻¹ and 1,403 cm⁻¹ are ν_{asym} (COO⁻) and ν_{sym} (COO⁻), respectively, which are all associated with the original oleate ligands. (b) J-V characteristics of ITO/PEI/PbSe NCs/PEI/Al electron-only devices. Solid lines represent the calculated J-V characteristics according to the conventional SCLC model. The PbSe NCs employed were 2.6 nm in size.

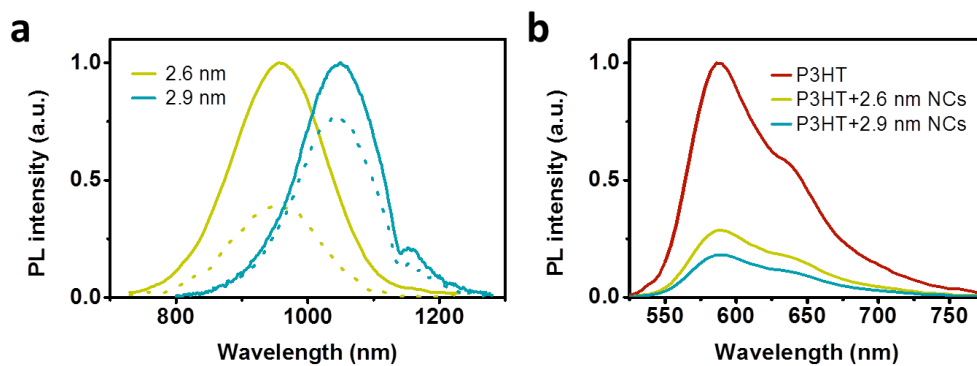


Figure 2. (a) PL spectra of PbSe NCs and PbSe:P3HT (1:1 wt% blend) solution in dichlorobenzene, excited at 680 nm. Solid lines represent normalized PL spectra of PbSe NC solutions of two different sizes, and dashed lines represent corresponding PL spectra for solutions blended with P3HT. (b) PL spectra of a P3HT solution and P3HT:PbSe (1:1 wt% blend) solutions in dichlorobenzene for 2 NC sizes, all excited at 405 nm.

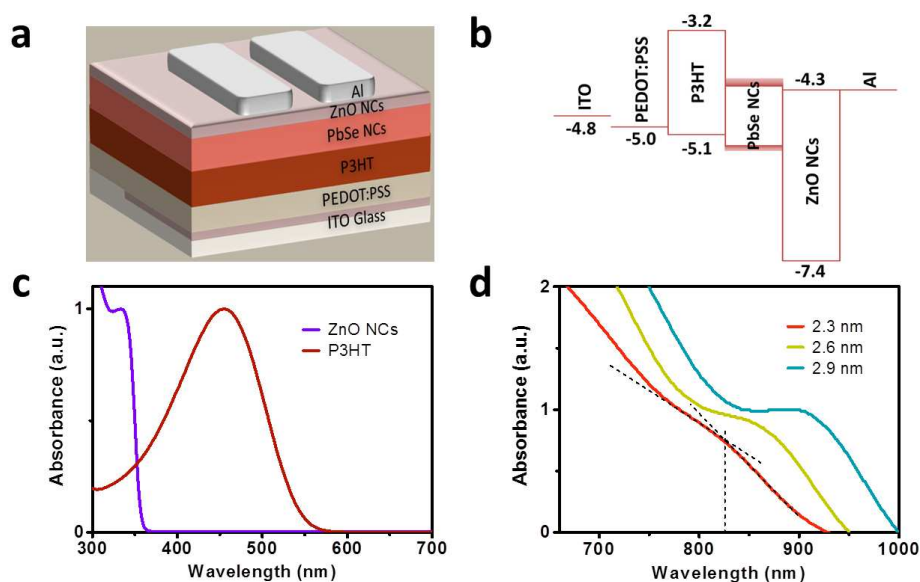


Figure 3. (a) Schematics of the planar HSC device based on P3HT and PbSe NCs, (b) energy level diagram of the device, (c) absorption spectra of ZnO NCs and P3HT, (d) absorption spectra of PbSe NCs of 3 different sizes indicated on the frame.

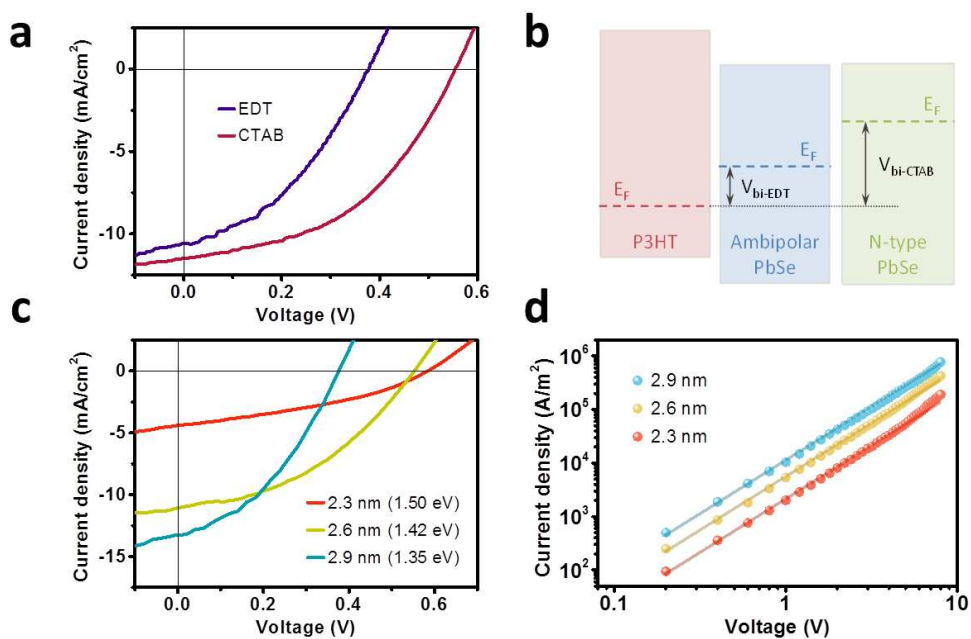


Figure 4. (a) J-V characteristics of HSCs based on 2.6 nm PbSe NCs treated with CTAB and EDT. (b) Energy band diagrams of P3HT/PbSe NC heterojunctions, where the PbSe NC films are either intrinsic or n-type doped. (c) J-V characteristic of HSCs based on PbSe NCs of 3 different sizes / bandgaps, as indicated on the frame. (d) J-V characteristics of ITO/PEI/PbSe NCs/PEI/Al electron-only devices employing different size PbSe NCs. Solid lines represent the calculated J-V characteristics according to the conventional SCLC model.

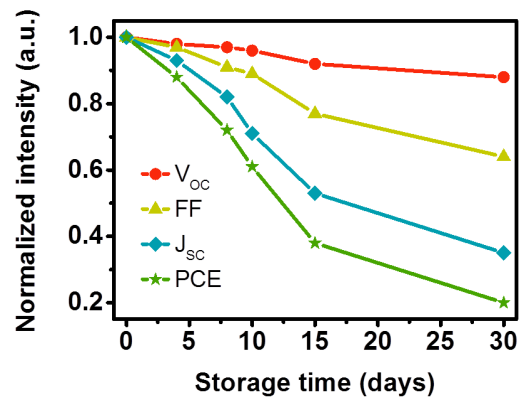


Figure 5. Time evolution of the photovoltaic performance parameters of the HSC devices stored in a N_2 -filled glove box.

TOC graph

